Progress In Electromagnetics Research, PIER 61, 253–270, 2006

DESIGN OF AN ACTIVE INTEGRATED ANTENNA FOR A PCMCIA CARD

F. Bilotti

University of ROMA TRE
Department of Applied Electronics
Via della Vasca Navale n° 84, 00146, Rome, Italy

F. Urbani

University of Texas at Brownsville
Department of Engineering
80 Fort Brown, Brownsville, TX 78520, USA

L. Vegni

University of ROMA TRE
Department of Applied Electronics
Via della Vasca Navale n° 84, 00146, Rome, Italy

Abstract—This paper presents the design and implementation of an Active Integrated Antenna (AIA) using a Voltage Controlled Oscillator (VCO) for applications in the Industrial Scientific Medical band (2.4 ÷ 2.4835 GHz). Surface Mounting Device (SMD) technology has been applied in the realization of the passive and active components, and low cost FR-4 dielectric slabs have been employed for the integration of the antenna and the active/transmissive circuits, residing, respectively, on the opposite faces of a Personal Computer Memory Card International Association (PCMCIA) card. The proposed layout makes use of a properly corrugated ground plane, i.e., a High Impedance Ground Plane (HIGP), to improve the antenna performances and to minimize the coupling between the radiating component and other possible radiating elements and/or electronic circuits residing nearby. The analysis and the design of the radiating element with the HIGP are based on a rigorous full wave Method of Moment (MoM) formulation developed in the Spectral Domain (SD), while the design of the active circuitry is developed through the commercial tool AWR Microwave Office. The final design of the component is obtained hybridizing the

two methods and applying a Genetic Algorithm (GA) optimization tool in order to take advantage of the HIGP, while keeping the geometrical dimensions of the antenna suitable for mounting on a PCMCIA card, and maintaining the antenna performances acceptable. The measured results show the performances of the VCO, an antenna gain of 19.4 dBi and an increased front-to-back radiation ratio compared to the one of the same antenna mounted on a standard Perfect Electric Ground Plane (PEGP). This result, thus, demonstrates the minimization of the interferences between the designed antenna and other possible radiating and transmissive devices residing nearby.

1. INTRODUCTION

Integrated Antennas and Active Integrated Antennas (AIAs) are widely used in the area of wireless communications, both for civilian and military purposes. The success of such devices is mainly due to their low cost, low profile, good compatibility with integrated circuits, great conformability on curved surfaces and reduced space occupancy (see [1–6] and references therein). In particular, AIAs are devices in which a passive antenna element and an active circuitry are integrated together on the same substrate [1]. The integration of active solid state devices like oscillators, amplifiers, and mixers grants greater compactness, lower costs and higher power efficiencies with respect to conventional passive layouts [1].

The design of such components may involve several aspects related to different areas of microwave and millimeter-wave engineering, among which fabrication technology and material characterization. In addition, the design is complicated by some non-trivial issues arising when considering the combination of active elements with Radio Frequency (RF) circuits and radiating components. For instance, active components may affect the behavior of passive structures, so that a trade off is often necessary between the radiating and the guiding structure performances [2, 5, 6] of AIAs. Moreover, another issue to be addressed in the design of AIAs is the undesired radiation due to the active devices, which should be eliminated without affecting the other features of the component. Finally, active devices always present undesired higher-order harmonics, which should be suppressed through properly designed filtering circuits [7–9].

All these aspects are addressed in the design proposed in the following. The antenna has been intended to work in the Industrial Scientific Medical (ISM) band ($2.4 \div 2.4835$ GHz) and makes use of a Voltage Controlled Oscillator (VCO). Surface Mounting Device (SMD)

technology has been used for the realization of passive and active components and the overall structure has been integrated in a low cost FR-4 dielectric slab. The final layout consists of a bi-level structure, in which the radiating element is positioned on the opposite face with respect to the active circuit and the total dimensions fit in a Personal Computer Memory Card International Association (PCMCIA) card. Since the two different levels of the structure are separated by a copper ground plane, the designs of the active/passive circuitry and of the antenna module are almost independent from each other. In addition, the presence of the ground plane effectively reduces the interference caused by the active circuitry on the passive radiating element (and vice versa).

Antennas working in the ISM band should not interfere with other possible radiating elements working in the same band and mounted on the same chassis (e.g., a Wi-Fi antenna and a Bluetooth antenna mounted on the same laptop). In order to reduce such mutual interactions, a properly designed set of periodic corrugations has been added into the antenna module. Such corrugations, which create a High Impedance Ground Plane (HIGP) [10, 11], allow minimizing the surface wave contribution, which is responsible for undesired coupling effects and lowers the radiation efficiency of the antenna. In addition, such periodic structures behave as magnetic conductors in certain frequency ranges and, thus, are found to be effective as reflectors to improve the radiation features of horizontal antennas [10, 11].

It has been recently shown that the design of a radiating element backed by an HIGP cannot be studied independently from the design of the HIGP itself [12], due to the strong mutual interactions between the electrical image of the antenna with respect to the ground plane and the antenna itself. Therefore, a proper optimization technique, based on the Genetic Algorithms (GAs) [13], has been employed to optimize the overall antenna module (radiating element + HIGP). The analysis tool is based on the Spectral Domain (SD) full-wave analysis [14] together with a Method of Moment (MoM) numerical technique [15]. For what concerns the passive and active circuitries, instead, they have been designed through AWR Microwave Office, which is a commercial tool employing harmonic balance techniques for the analysis and synthesis of RF non linear circuits.

The structure of the paper is as follows: in Section 2 an overview of the proposed AIA design is given in terms of an overall comprehensive block diagram. Section 3 treats the synthesis of the active and passive circuitry residing on the back layer of the card and the corresponding measured results. In Section 4 the design of the antenna and of the HIGP residing in the top level of the structure is presented

together with some numerical and experimental results showing the main features of the proposed antenna.

2. OVERVIEW OF THE PROPOSED AIA

The equivalent block diagram of the AIA designed in the paper is shown in Fig. 1. The antenna is located in the most right part of the diagram and is fed by a RF signal coming through some buffer and matching network stages.

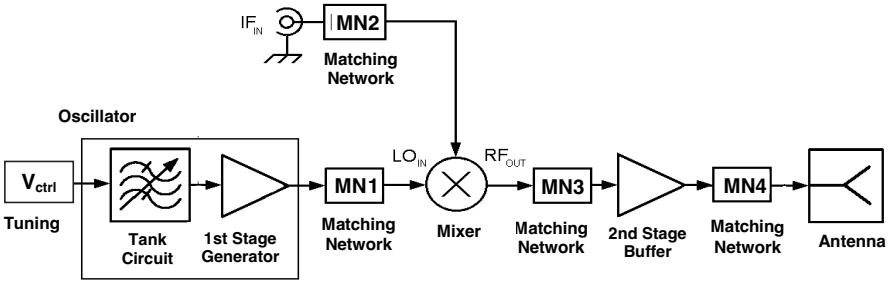

Figure 1. Equivalent block diagram of the designed AIA.

The local oscillator is designed to work in the S band ($2 \div 4\,\text{GHz}$) and the mixer converts an Intermediate Frequency (IF) signal into the RF stream feeding the antenna input. The working frequency of the local oscillator is set to $f_{LO} = 2.33\,\text{GHz}$, while the IF frequency is set to $f_{IF} = 110\,\text{MHz}$, so that the corresponding RF signal has a beat at $f_{RF} = f_{LO} + f_{IF} = 2.44\,\text{GHz}$, with a conversion loss of 6 dB.

Some buffer stages and matching networks have been also added for the proper operation of the device.

In the following sections we will present the details of the design of these elements.

3. DESIGN OF THE ACTIVE AND PASSIVE CIRCUITRY

3.1. Circuit Description

The implementation of the oscillator module is depicted in Fig. 2. The tank circuit in the middle is a common band-pass filter that determines the oscillation frequency. It has been realized using a varactor, whose capacitance is controlled by the external DC voltage indicated in Fig. 1 as V_{ctrl}, allowing for an electronic tuning of the oscillation

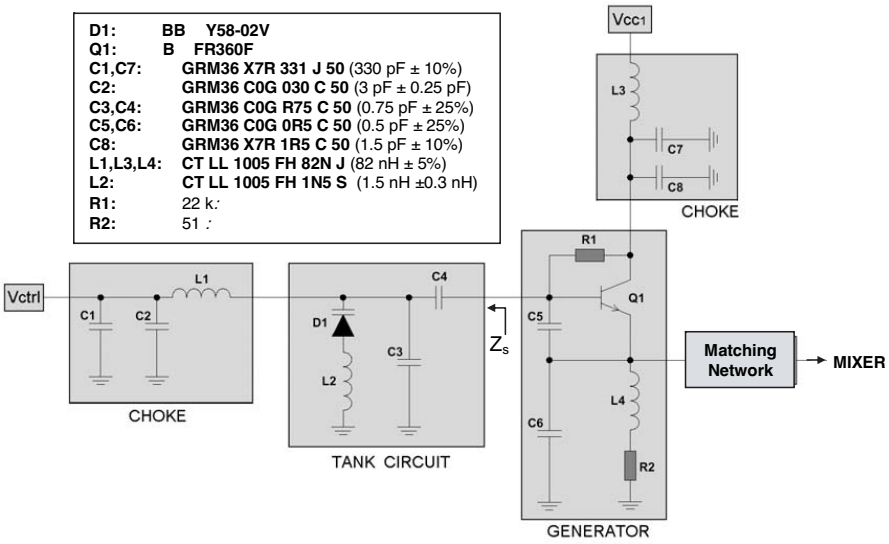

Figure 2. Implementation of the oscillator module. The employed components are reported in the inset.

frequency. In order to assure the DC voltage transfer to control the varactor capacitance and the isolation of the V_{ctrl} power supply from RF signals, a proper *choke circuit* using a series inductor and two shunt capacitances has been added before the tank circuit. Finally, the *generator* block is formed by a high frequency Bipolar Junction Transistor (BJT) in the emitter follower configuration connected to a second *choke circuit* capable of shorting out the RF signals from the BJT collector. The inductor L_4 prevents the RF signals from flowing to the ground through the DC network.

The *mixer module* is a MMIC Double-Balanced Mixer commonly used for RF communications (U2795B), which exhibits good performances in terms of attenuation, conversion gain, linearity, Third Order Intercept Point (OIP3), Third Order Input Intercept Point (IIP3), isolation, etc., and last but not least the cost factor.

The *buffer module* consists of a RF amplifier with proper matching cells and a choke circuit for the bias, as shown in Fig. 3.

The RF amplifier has a twofold function as stage of separation: it reduces the antenna load effect on the mixer oscillator and it increases the radiated power. The input matching network is realized simply through a by-pass capacitance, while the output matching network is realized using a resistive PAD, whose element values are adjusted

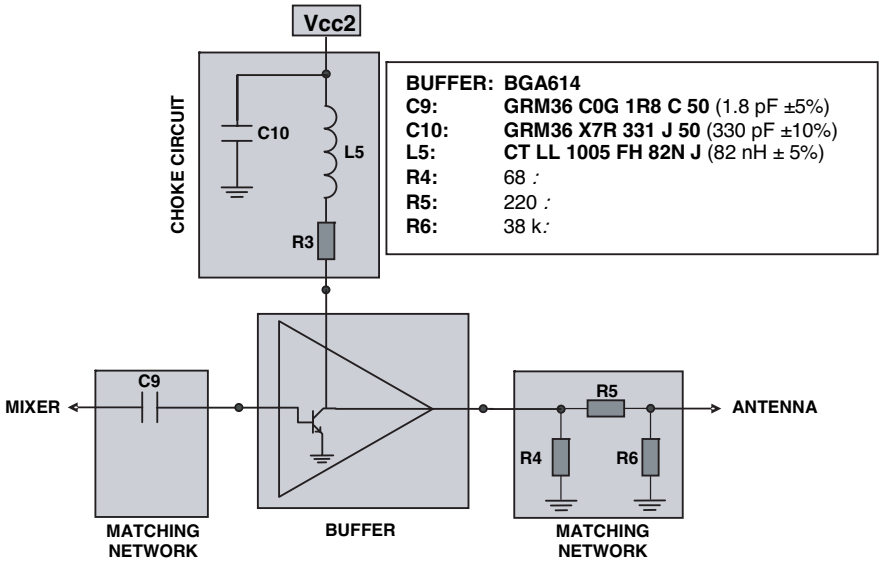

Figure 3. Implementation of the buffer module with its matching networks. The used components are reported in the inset.

at the end of the design process. This allows, during the calibration phase, both optimizing the device performances and compensating any undesired effect resulting from tool tolerances, material imperfections, packaging, and modeling accuracy.

Finally, in order to suppress the undesired higher-order harmonics coming from the active devices, the non uniform transmission line transition already designed by the authors and reported in [16] has been connected between the last matching network and the antenna. For the details on the design of this tapered matching line we remand to [16].

3.2. VCO Measured Results

The key point in the design of the active circuitry presented in the previous sub-section is represented by the design of the VCO. The method of the Negative Differential Resistance (NDR) [17, 18] has been applied for designing the oscillator module and its actual operation has been tested through the measurements made on a realized prototype of the antenna. In Fig. 4 the comparison between measured and simulated VCO oscillation frequencies is plotted as a function of V_{ctrl}. The measured power levels in dBm have been also added in the graphs.

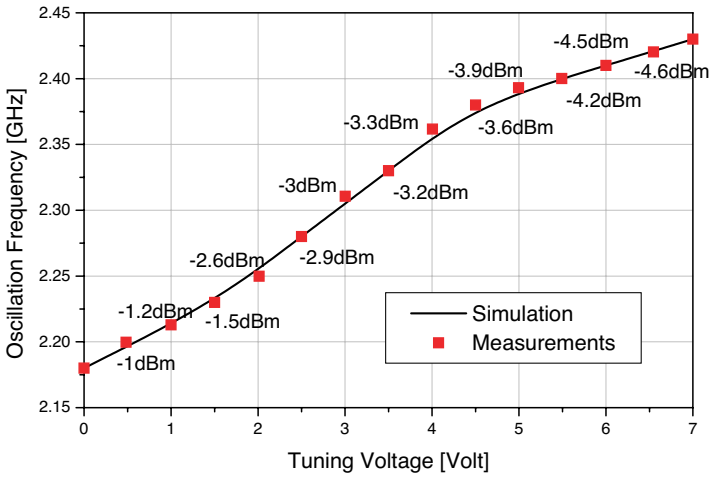

Figure 4. Comparison between measured and simulated VCO oscillation frequencies as a function of the tuning voltage. The simulation, performed through AWR Microwave Office, exploits the data sheet of the components described in the insets of Figs. 2–3 and takes into account also the effects of the packaging. The measured output power levels have been also reported.

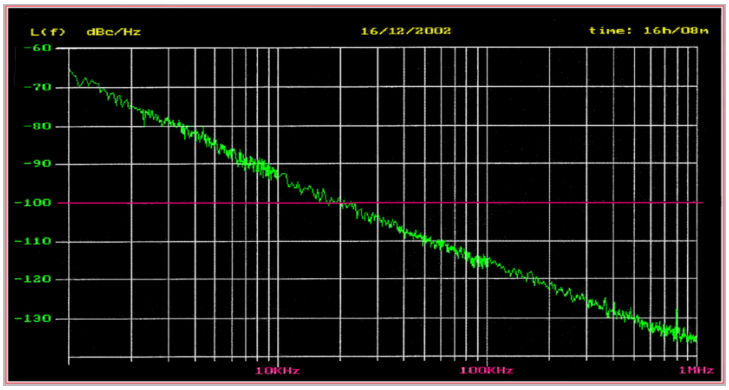

Figure 5. Measured phase noise of the oscillator.

The phase noise of the oscillator has been also measured and the result is reported in Fig. 5. The obtained values of the phase noise (-90 dBc/Hz at 10 kHz and -110 dBc/Hz at 100 kHz) are pretty acceptable for the proposed application.

4. DESIGN OF THE ANTENNA MODULE

4.1. Proposed Antenna Layout

The radiating element is a patch antenna working at the central operating frequency $f_{RF} = 2.44\,\text{GHz}$ of the ISM band. In order to reduce the surface wave radiation of the antenna, which is a relevant point to decrease the electromagnetic influence on the other microwave circuits located nearby, a two-layer HIGP [10] made of a double grid of squared metallic mushrooms disposed in a periodical pattern has been designed.

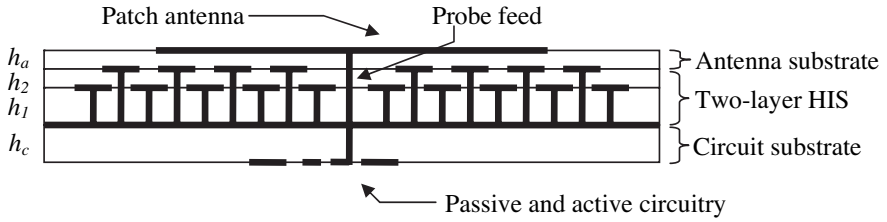

Figure 6. Geometry of the physical structure implementing the AIA block diagram of Fig. 1 (the thicknesses of the layers are not in scale).

The physical structure which implements the block diagram of Fig. 1 is reported in Fig. 6. It consists of four layers: the bottom layer is a FR-4 dielectric slab hosting the passive and active circuitry; the two layers in the middle are the two FR-4 dielectric slabs corresponding to the HIGP; the top layer is made by air and represents the antenna substrate. The bottom layer is separated from the three antenna layers above (HIGP + radiating element) by a metallic ground plane, while the radiating element is fed by the inner conductor of a coaxial probe. The coaxial pin is directly soldered to the end of the tapered microstrip line acting as the harmonic suppresser (see previous section and [16]) and there is no need of a proper transition, due to the small thickness of the substrate where the active circuit resides ($h = 1\,\text{mm}$).

The analysis of the radiating element may be performed through different approximate and rigorous methods [19]. We have assumed the metallizations as infinitely thin and perfectly conducting, and we have applied the rigorous analysis method based on the Electric Field Integral Equation (EFIE). Imposing the boundary condition for the

electric field on the metallic surfaces, the EFIE is obtained as follows:

$$-\hat{\boldsymbol{z}} \times \boldsymbol{E}^{inc}(\boldsymbol{r}_{met}) = \hat{\boldsymbol{z}} \times \int\limits_{S'_{met}} \underline{\boldsymbol{G}}(\boldsymbol{r}_{met}|\boldsymbol{r}') \cdot \boldsymbol{J}(\boldsymbol{r}') dS'_{met}, \quad \boldsymbol{r}_{met}, \boldsymbol{r}' \in S_{met} \tag{1}$$

$\boldsymbol{E}^{inc}(\boldsymbol{r})$ is the incident field produced by the impressed source (i.e., the coaxial probe), S_{met} is the surface of the metallizations (HIGP + patch), $\boldsymbol{r}'$ is the source vector, $\boldsymbol{r}_{met}$ is the vector describing the points on all the metallic surfaces, $\underline{\boldsymbol{G}}(\boldsymbol{r}|\boldsymbol{r}')$ is the spatial domain dyadic Green's function of the grounded slab (without metallizations), $\boldsymbol{J}(\boldsymbol{r}')$ is the induced current density on the patch, and $\hat{\boldsymbol{z}}$ is the unit vector of the vertical axis.

Equation (1) is an integral equation in the unknown vectorial function $\boldsymbol{J}(\boldsymbol{r}')$. The solution of this equation is performed here in the SD, where the Green's dyad of the isotropic grounded slab may be expressed in closed form [20], and is demanded to a Method of Moments (MoM) numerical tool [21–23], employing regular roof-top basis functions [22]. Due to the small metallizations of the HIGP, the number of unknowns rapidly increases with the extension of the HIGP itself, and, thus, an acceleration technique is needed. The authors have recently extended the formulation in [22] for the semi-analytical evaluation of the entries of the MoM impedance matrix also to the entries of the excitation vector [23]. This formulation is based on the asymptotic Green's function of the grounded slab and allows an increasing computational time saving as the number of unknowns increases [23].

The shorting posts connecting the metallizations and the metallic plate of the HIGP, have been modeled and added in the MoM matrix through the formulation reported in [21] (and references therein). The mutual interactions between both the shorting pins and the patches of the mushroom structure, thus, are fully taken into account in the MoM numerical solution.

Since the behavior of an integrated antenna above an HIGP is affected by the mutual interactions between the radiating element and the metallic corrugations of the ground plane, it is not practical to design the antenna and the HIGP as two separate units [12].

As a matter of fact, in order to achieve the desired electrical and radiating features, the final antenna element should result from an optimization procedure, applied contemporarily to the design of both the radiating element and the two-layer HIGP. The starting iteration stage of this procedure is given by the set of the geometrical parameters obtained when the radiating element (with a PEGP) and the two-layer HIGP are designed independently in order to work in

the required frequency band. Then, a classic GA [13] is used to adjust the geometrical parameters so that the antenna matches the desired requirements.

4.2. Design of the Radiating Element for the Iteration Starting Procedure

The reference radiating element to be used in the first step of the GA optimization has been obtained from the design proposed in [24] for GSM terminals, changing the dimensions of both the ground plane and the patch to assure that the antenna operates properly in the desired IMS frequency band (see Fig. 7).

This antenna has a finite electric ground plane with the typical dimensions of a PCMCIA card. Due to the finite size of the ground plane, the EFIE (1) applies both to the radiating element and to the ground plane, leading to a final number of 614 unknowns[†].

The matching features, the antenna gain as a function of frequency, and the radiation pattern at the central operating frequency $f_{RF} = 2.44\,\text{GHz}$, reported in Fig. 7b–7e show the effectiveness of the designed radiating element to work in the ISM band. Anyway, the back-radiation of the antenna is still not satisfying (see Fig. 7d) because of the surface wave radiation, which is also responsible of some of the undesired coupling with other components in close proximity.

It is worth noting that the results in Fig. 7b–7e have been obtained without considering the effects of the active circuit, since it is separated from the radiating element by the ground plane. Therefore, the antenna gain reported in Fig. 7c refers only to the antenna element by itself.

4.3. Design of the HIGP for the Starting Iteration Stage

The geometry of the unit cell of the periodic two-layer HIGP designed to work in the band $2.4 \div 2.4835\,\text{GHz}$ is reported in Fig. 8.

Following [10], a lossless bi-layer HIGP can be in first approximation represented through its reactive surface impedance, which is given by:

$$Z_s(\omega) = j\frac{\omega L}{1-\omega^2 LC} \tag{2}$$

where ω is the angular frequency and L and C are the equivalent capacitance and inductance, respectively, associated to the periodic structure. At the resonant frequency $f_0 = 1/(2\pi\sqrt{LC})$ the HIGP

[†] The results shown in Figs. 7b–7e have been obtained simulating 30 frequency points in 2 minutes and 15 seconds on a Pentium 4, 2 GHz CPU, 512 Mb RAM.

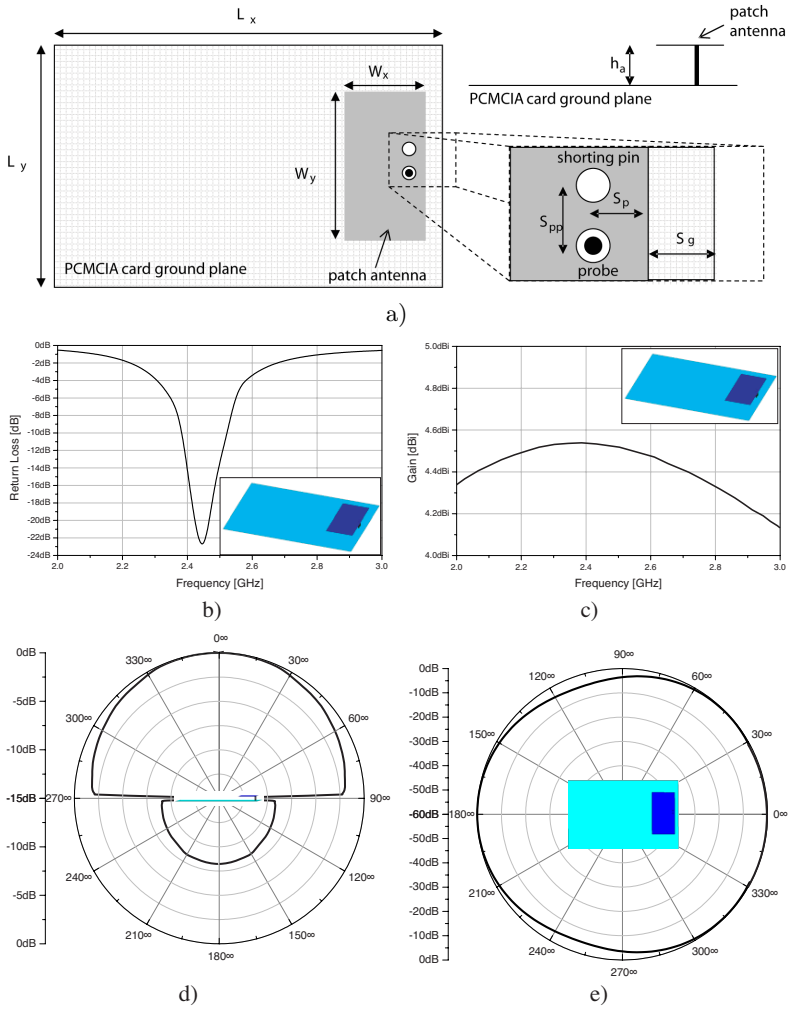

Figure 7. Layout and electromagnetic features of a patch antenna mounted on a regular metallic ground plane for a PCMCIA card. a) Antenna layout. The geometrical parameters are: $L_x = 60\,\text{mm}$, $L_y = 40\,\text{mm}$, $W_x = 12.4\,\text{mm}$, $W_y = 24\,\text{mm}$, $S_{pp} = 1.5\,\text{mm}$, $S_p = 1\,\text{mm}$, $S_g = 3\,\text{mm}$, $h_a = 3\,\text{mm}$. The antenna is printed on a 0.2 mm thick FR-4 slab ($\varepsilon_r = 4.4, \tan\delta = 0.02$) and the radii of both the shorting pin and the probe are 0.3 mm. b) Return Loss of the antenna at the input port as a function of frequency. c) Gain of the antenna as a function of frequency. d) Elevation radiation pattern of the antenna at the central frequency of operation: 2.44 GHz. e) Azimuthal radiation pattern of the antenna at the central frequency of operation: 2.44 GHz.

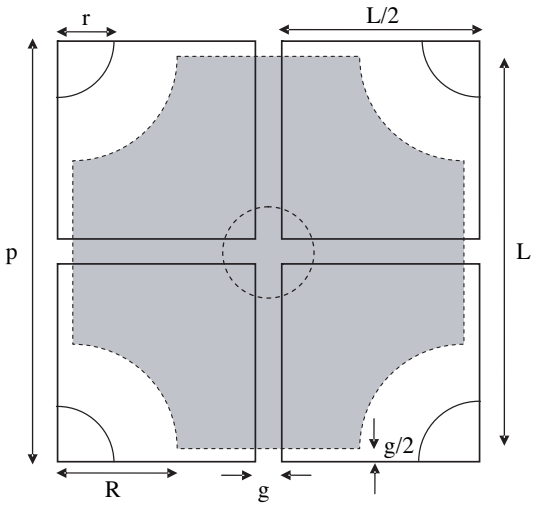

Figure 8. Geometry of the unit cell of the periodic two-layer HIGP. The shaded patch refers to the lower level, while the empty patches refer to the upper layer. Note that the upper patches have a squared geometry, while the lower patches are identical to the upper ones, but with rounded corners created to accommodate the vias supporting the upper patches. The geometrical parameters are: $p = 3.05\,\text{mm}$, $L = 3\,\text{mm}$, $g = 0.05\,\text{mm}$, $r = 0.4\,\text{mm}$, $R = 0.8\,\text{mm}$. The thicknesses of the substrates are: $h_1 = 1.4\,\text{mm}$, $h_2 = 0.12\,\text{mm}$.

behaves like a perfect magnetic conductor and does not support surface wave propagation. Far from the resonant frequency, instead, it resembles a PEGP ($Z_s(\omega) \cong 0$). Moreover, around the resonance frequency the behavior of the HIGP is that of a reactive surface (inductive below the resonance and capacitive beyond the resonance).

The equivalent parameters L and C depend on the geometrical dimensions of the unit cell in Fig. 8 and on the constitutive parameters of the dielectric bi-layer and are given by:

$$C = \varepsilon_2 \frac{A}{h_2} \qquad L = \mu_1 h_1 \tag{3}$$

where μ_1 is the permeability of the first layer, ε_2 is the permittivity of the second layer, and A is the overlapping area between the metallizations of the two layers in the unit cell of Fig. 8. Using equations (3) and the further constraint $1/(2\pi\sqrt{LC}) = 2.44\,\text{GHz}$, the design of the bi-layer HIGP is a straightforward matter. The

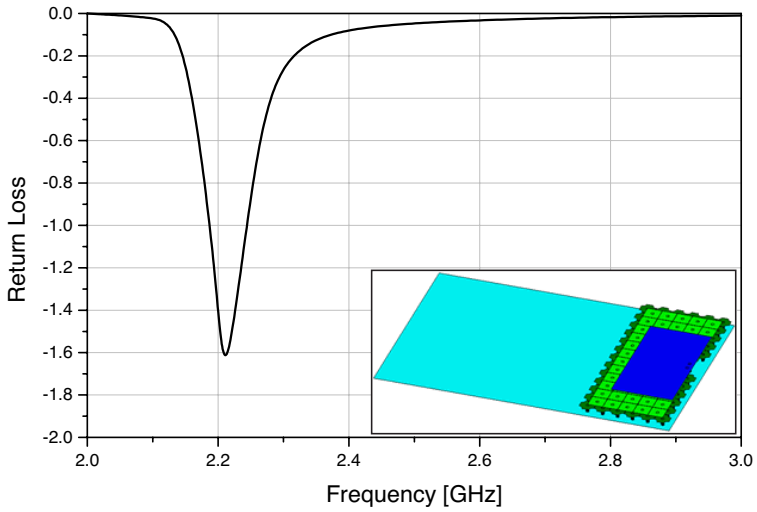

Figure 9. Return Loss as a function of frequency of the antenna depicted in Fig. 7a when backed by a HIS whose unit cell is depicted in Fig. 8. For the geometrical parameters you may refer to the captions of Fig. 7 and Fig. 8. As depicted in the inset, the HIGP is realized by a 5×12 double layer mushroom structure.

corresponding geometrical parameters are reported in the caption of Fig. 8.

4.4. Results of the Optimized Antenna

Once the antenna and its HIGP have been designed independently to work at the desired frequency, the synthesis of the antenna module is not completed, but the following optimization technique should be performed.

- In the first iteration stage the PEGP is removed from the antenna of Fig. 7a and the radiating element is directly backed by the HIGP, whose unit cell is reported in Fig. 8. The analysis in this case is time consuming, because we need to impose the boundary condition of the tangential electric field not only on the radiating patch and on the finite size ground plane, but also on all the metallic corrugations of the HIGP. The accurate MoM numerical analysis of the antenna now requires 13864 unknowns and around half an hour for the overall simulation of 30 frequency points on the same Pentium 4 as before. The resulting return loss at the input port has been reported in Fig. 9. The result is that the operating

frequency is shifted towards lower frequencies, while the matching features are degraded with respect to those reported in Fig. 7. This result is in line with the theory presented in [12], and shows again that the design of a patch antenna backed by a HIGP needs further consideration.

- The second step of the design consists in reducing the thickness of the antenna substrate to take advantage of using an HIGP near its resonance and, finally, in adjusting iteratively the geometrical dimensions of both the HIGP corrugations and the radiating element, so that a prescribed requirement is achieved. The constraint used here was a return loss less than -10 dB within the ISM frequency band. This iteration stage is not viable through a trial and error approach, because the time required for each MoM full-wave simulation is very long and the amount of the employed memory is very extensive. To overcome this limitation, a GA search has been integrated in the MoM code as in [13], employing the following fitness function to be minimized:

$$\text{fitness} = \sqrt[N_f]{\prod_{i=1}^{N_f}(-20\log_{10}|S_{11}(f_i)|)}$$

where N_f is the number of the simulated frequency points in the ISM band. Applying this optimization tool, the structure is simulated only once (i.e., at the first iteration, as reported in the previous point), while the next configurations, obtained varying the geometrical dimensions, do not need to be simulated again through an extensive MoM simulation (see [13] and references therein).

The electrical and radiating features of the optimized antenna are reported in Figs. 10a–10e, together with the new geometrical dimensions of both the HIGP and the radiating element. The new antenna backed by the HIGP is smaller and thinner compared to the one depicted in Fig. 7 backed by a standard metallic ground plane. In addition, results in Fig. 10a and Fig. 10b show that both the matching features and the gain are improved with respect to a standard metallic backing. These results may be explained also using the theory reported in [25], where it is pointed out that the new corrugated structure behaves mostly like an inductive surface, than an AMC. In line with [26], this surface is able to reduce the near-field radiation, which is responsible of the reduced back-radiation, as reported in Fig. 10c, and of the reduced interference with possible other circuits residing nearby.

The two antennas here considered, one with the standard metallic ground plane (Fig. 7) and the other with the HIGP (Fig. 10), have been

simulated so far as if independent on the active circuit residing on the back layer of the structure. However, the measurements made on the realized prototype do not differ significantly from the results reported in Fig. 7 and in Fig. 10, apart from the maximum broadside gain, which has been measured to be 18.6 dBi and 19.4 dBi, respectively, at the central operating frequency $f_{RF} = 2.44$ GHz.

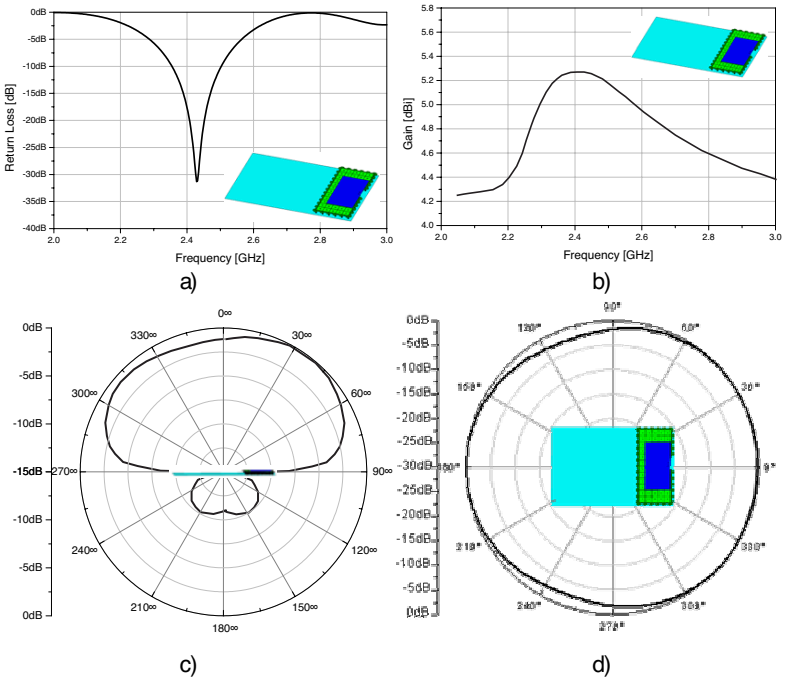

Figure 10. Electromagnetic features of the optimized patch antenna mounted on an HIGP for a PCMCIA card. The geometrical parameters characterizing the antenna are: $L_x = 60$ mm, $L_y = 40$ mm, $W_x = 10.8$ mm, $W_y = 21.6$ mm, $S_{pp} = 1.28$ mm, $S_p = 1$ mm, $S_g = 3$ mm, $h_a = 1.7$ mm. The geometrical parameters of the HIGP are the ones reported in the caption of Fig. 8, but $p = 2.95$ mm and $L = 2.9$ mm. The antenna is printed on a 0.2 mm thick FR-4 slab ($\varepsilon_r = 4.4$, $\tan\delta = 0.02$) and the radii of both the shorting pin and the probe are 0.3 mm. a) Return Loss of the antenna at the input port as a function of frequency. b) Gain of the antenna as a function of frequency. c) Elevation radiation pattern of the antenna at the central frequency of operation: 2.44 GHz. d) Azimuthal radiation pattern of the antenna at the central frequency of operation: 2.44 GHz.

5. CONCLUSIONS

An active integrated antenna for PCMCIA cards has been presented in this paper. The active antenna makes use of a VCO and has been realized through the SMD technology. The design of the active circuit has been conducted through AWR Microwave Office and has been mainly focused on the oscillator module. The experimental results have confirmed the effectiveness of the designed VCO in terms of both oscillation frequency versus the tuning voltage, and phase noise.

The antenna element has been realized applying the HIGP technology to minimize the interactions with possible other microwave components residing nearby, in order to increase the antenna gain and to reduce the antenna size. All these goals have been achieved and the resulting measured broadside gain of the antenna has been found to be 19.4 dBi at the central operating frequency $f_{RF} = 2.44$ GHz, maintaining the radiation pattern and the matching features compatible with a PCMCIA card operation.

REFERENCES

1. Lin, J. and T. Itoh, "Active integrated antennas," *IEEE Trans. Microwave Theory Tech.*, Vol. MTT-42, No. 12, 2186–2194, Dec. 1994.
2. Pobanz, C. W. and T. Itoh, "Active integrated antennas," *IEEE Potentials*, Vol. 16, No. 2, 6–10, April–May 1997.
3. Itoh, T., "Active integrated antennas for wireless applications," *Proc. Microwave Conference APMC '97, 1997 Asia-Pacific*, Vol. 1, 309–312, Dec. 2–5, 1997.
4. Qian, Y. and T. Itoh, "Progress in active integrated antennas and their applications," *IEEE Trans. Microwave Theory Tech.*, Vol. MTT-46, No. 11, 1891–1900, Nov. 1998.
5. Chang, K., R. A. York, P. S. Hall, and T. Itoh, "Active integrated antennas," *IEEE Trans. Microwave Theory Tech.*, Vol. MTT-50, No. 3, 937–944, Mar. 2002.
6. Leong, K. M. K. H. and T. Itoh, "Developments in active integrated antennas," *Proc. 2003 IEEE Antennas Propagat. Society Int. Symp.*, Vol. 1, 212–215, June 22–27, 2003.
7. Kwon, S., B. M. Lee, Y. J. Yoon, W. Y. Song, and J. G. Yook, "A harmonic suppression antenna for an active integrated antenna," *IEEE Microwave Wireless Compon. Lett.*, Vol. 13, No. 2, 54–56, Feb. 2003.
8. Erturk, B., R. G. Rojas, and P. Roblin, "Hybrid analysis/design

method for active integrated antennas," *IEE Proc. Microwaves Antennas Propagat.*, Vol. 146, No. 2, 131–137, Apr. 1999.

9. Anzellotti, E., F. Bilotti, and L. Vegni, "Broad-band tuning of an AIA amplifier using 1-D PBG transmission lines," *J. Electromag. Waves Applicat.*, Vol. 17, No. 4, 571–584, 2003.
10. Sievenpiper, D., L. Zhang, R. F. J. Broas, N. G. Alexopoulos, and E. Yablonovitch, "High-impedance electromagnetic surface with a forbidden frequency band," *IEEE Trans. Microwave Theory Tech.*, Vol. MTT-47, No. 11, 2059–2074, Nov. 1999.
11. Yang, F. R., K. P. Ma, Y. Qian, and T. Itoh, "A uniplanar compact Photonic-BandGap (UC-PBG) structure and its applications for microwave circuits," *IEEE Trans. Microwave Theory Tech.*, Vol. MTT-47, No. 8, 1509–1514, Aug. 1999.
12. Bilotti, F., A. Alù, and L. Vegni, "Analysis of dipole and patch radiators in presence of artificial magnetic and impedance reflectors and ground planes: Preliminary results," *Proc. PIERS'04, CD-Digest*, 28–31, Mar. 2004.
13. Bilotti, F., L. Vegni, and F. Urbani, "Synthesis of patch sntennas loaded by inhomogeneous dubstrates via a combined spectral domain — Genetic Algorithm Approach," *Microwave and Optical Technology Letters*, Vol. 39, No. 6, 464–468, Dec. 20, 2003.
14. Vegni, L., R. Cicchetti, and P. Capece, "Spectral dyadic Green's function formulation for planar integrated structures," *IEEE Trans. Antennas Propagat.*, Vol. AP-36, No. 8, 1057–1065, Aug. 1988.
15. Bilotti, F. and C. Vegni, "Rigorous and efficient full-wave analysis of trapezoidal patch antennas," *IEEE Trans. Antennas Propagat.*, Vol. AP-49, No. 12, 1773–1776, Dec. 2001.
16. Urbani, F., F. Bilotti, and L. Vegni, "Synthesis of filtering structures for microstrip active antennas using Orlov's formula," *ETRI Journal*, Vol. 27, No. 2, 166–171, Apr. 2005.
17. Vendelin, G. D., A. M. Pavio, and U. L. Rohde, *Microwave Circuit Design Using Linear and Nonlinear Techniques*, Wiley, New York, 1990.
18. Kurokawa, K., "Some basic characteristics of broadband negative resistance oscillator circuits," *Bell Syst. Tech. J.*, No. 8, 1937–1955, 1969.
19. Pozar, D. M., "Microstrip antennas," *Proc. IEEE*, Vol. 80, No. 1, 79–91, Jan. 1992.
20. Vegni, L., R. Cicchetti, and P. Capece, "Spectral dyadic Green's function formulation for planar integrated structures," *IEEE*

Trans. Antennas Propagat., Vol. 36, No. 8, 1057–1065, Aug. 1988.

21. Waterhouse, R. B., "The use of shorting posts to improve the scanning range of probe-fed microstrip patch phased arrays," *IEEE Trans. Antennas Propagat.*, Vol. 44, No. 3, 302–309, Mar. 1996.
22. Park, S., C. A. Balanis, and C. R. Birtcher, "Analytical evaluation of the ssymptotic Impedance matrix of a grounded dielectric slab with roof-top functions," *IEEE Trans. Antennas Propagat.*, Vol. AP-26, No. 2, 251–259, Feb. 1998.
23. Bilotti, F., A. Alù, F. Urbani, and L. Vegni, "Asymptotic evaluation of the MoM excitation vector for probe-fed microstrip antennas," *J. Electromag. Waves Applicat.*, Vol. 19, No. 12, 1639–1654, 2005.
24. Hsiao, F. R. and K. L. Wong, "A shorted patch antenna with an l-shaped ground plane for internal mobile handset antennas," *Microw. Opt. Technol. Lett.*, Vol. 33, No. 4, 314–316, May 20, 2002.
25. Mosallaei, H. and K. Sarabandi, "Antenna miniaturization and bandwidth enhancement using a reactive impedance substrate," *IEEE Trans. Antennas Propagat.*, Vol. AP-52, No. 9, 2403–2414, Sept. 2004.
26. Tretyakov, S. A. and C. R. Simovski, "Wire antennas near artificial impedance surfaces," *Microw. Opt. Technol. Lett.*, Vol. 27, No. 1, 46–50, Oct. 5, 2000.